

Article

## A Pt-Doped TiO<sub>2</sub> Nanotube Arrays Sensor for Detecting SF<sub>6</sub> Decomposition Products

Xiaoxing Zhang <sup>1,\*</sup>, Jing Tie <sup>1</sup> and Jinbin Zhang <sup>1,2</sup>

<sup>1</sup> State Key Laboratory of Power Transmission Equipment & System Security and New Technology, Chongqing University, Shapingba District, Chongqing 400044, China;

E-Mails: cherrytie0123@hotmail.com (J.T.); Zhangjinbin023@126.com (J.Z.)

<sup>2</sup> Chongqing Power Company, Beibei, Chongqing 400700, China

\* Author to whom correspondence should be addressed; E-Mail: zhxx@cqu.edu.cn;

Tel.: +86-136-4055-1418; Fax: +86-23-6511-1935.

Received: 16 September 2013; in revised form: 18 October 2013 / Accepted: 22 October 2013 /

Published: 30 October 2013

---

**Abstract:** The detection of partial discharge and analysis of SF<sub>6</sub> gas components in gas-insulated switchgear (GIS) is important for the diagnosis and operating state assessment of power equipment. The use of a Pt-doped TiO<sub>2</sub> nanotube arrays sensor for detecting sulfur hexafluoride (SF<sub>6</sub>) decomposition products is proposed in this paper. The electrochemical pulse deposition method is employed to prepare the sensor array. The sensor's response to the main characteristic gaseous decomposition products of SF<sub>6</sub> is evaluated. The gas sensing characteristic curves of the Pt-doped TiO<sub>2</sub> nanotube sensor and intrinsic TiO<sub>2</sub> nanotube arrays sensor are compared. The mechanism of the sensitive response is discussed. Test results showed that the Pt-doped nanoparticles not only change the gas sensing selectivity of the TiO<sub>2</sub> nanotube arrays sensor with respect to the main characteristic SF<sub>6</sub> decomposition products, but also reduce the operating temperature of the sensor.

**Keywords:** gas sensor; Pt doped; TiO<sub>2</sub> nanotube arrays; SF<sub>6</sub> decomposition products

---

### 1. Introduction

The excellent insulating and arc extinguishing properties of sulfur hexafluoride (SF<sub>6</sub>) gas greatly improve the dielectric strength when used as an insulating medium. SF<sub>6</sub> has been widely utilized in gas-insulated switchgear (GIS) [1–4]. The reliability of GIS equipment is very high, however, its

inevitable intrinsic defects continue to cause varying degrees of partial discharge (PD). Active gas produced by discharge accelerates insulation aging and corrosion of metal surfaces and may eventually lead to equipment failure. Many studies have shown that when a GIS insulation error occurs, the energy generated by discharge causes the SF<sub>6</sub> gas to decompose and generate SF<sub>4</sub>, SF<sub>3</sub>, SF<sub>2</sub>, and various low-fluorine sulfides. These low-fluoride sulfides react with trace moisture and the oxygen present in the SF<sub>6</sub> gas and generate SOF<sub>4</sub>, SOF<sub>2</sub>, SO<sub>2</sub>F<sub>2</sub>, SO<sub>2</sub>, HF, and other compounds [5,6]. The common methods used at present to detect and analyze SF<sub>6</sub> partial discharge decomposition products include gas chromatography and infrared absorption spectrometry, but all these methods are offline laboratory detection methods, and on-site detection with these methods is difficult to implement.

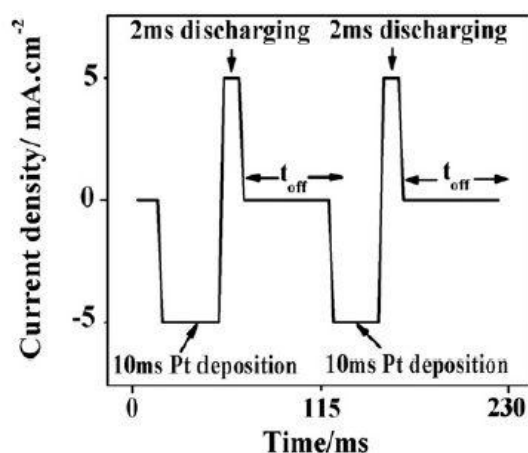
Titanium dioxide nanotube arrays (TiO<sub>2</sub>NTs) are typical 3D nanomaterials that have numerous interesting physical and chemical properties. These materials are inexpensive and can thus be employed in numerous applications [7]. Studies have shown that compared with other nanostructure forms TiO<sub>2</sub>NTs have a large specific surface area and produce interesting nano-sized effects. TiO<sub>2</sub>NTs are utilized in photocatalysis, sensors, solar cells, *etc.* and exhibit a huge potential for development, having become one of the major topics in international nanomaterial research [8]. Miniature gas sensors prepared with TiO<sub>2</sub>NTs exhibit a fast response and high sensitivity. Several scholars have made great progress in this area in recent years, and TiO<sub>2</sub>NTs sensors are utilized to test for O<sub>2</sub>, NO<sub>2</sub>, H<sub>2</sub>, ethanol gas, *etc.* as sensitive materials [9–11].

A Pt-doped TiO<sub>2</sub>NTs gas sensor prepared through a pulsed electrochemical deposition method based on intrinsic TiO<sub>2</sub>NTs is developed in this study. The sensor's capability to sense the major decomposition products of SF<sub>6</sub> is evaluated. Compared with the gas sensing properties of intrinsic TiO<sub>2</sub>NTs sensors, the Pt-doped nanoparticles change the gas sensing selectivity of the TiO<sub>2</sub>NTs sensor towards the main characteristic SF<sub>6</sub> decomposition products.

## 2. Experimental Section

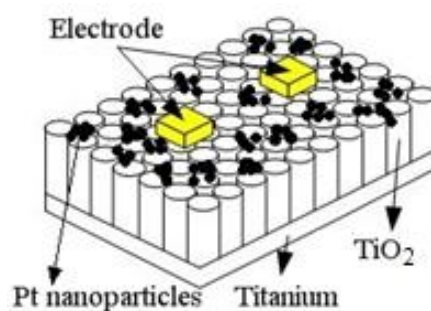
### 2.1. Preparation of Pt-Doped TiO<sub>2</sub>NTs

The preparation of the Pt-doped TiO<sub>2</sub>NTs was based on electrochemical deposition on intrinsic TiO<sub>2</sub>NTs. The TiO<sub>2</sub>NTs were prepared by anodic oxidation [12]. With a conventional three-electrode system, Pt-doped nanoparticles were deposited onto TiO<sub>2</sub>NTs by pulsed electrodeposition. In the three-electrode system, the prepared intrinsic TiO<sub>2</sub>NTs is the working electrode (geometric area of 4.0 cm<sup>2</sup>). A Ag/AgCl electrode is the reference electrode, and a platinum electrode is the counter electrode. Electronic pulse signals were provided by an Autolab PGSAT32 instrument (manufacturer, city, state abbrev if US, country) in potential (constant) control mode. The current–time curve of the Pt-doped TiO<sub>2</sub>NTs preparation is shown in Figure 1. The electrolytes were prepared with pH = 4.4 aqueous H<sub>2</sub>PtCl<sub>6</sub>·6H<sub>2</sub>O (1 g/L) and H<sub>3</sub>BO<sub>3</sub> (20 g/L) at 50 °C. The deposition time of the sample was set to 90 s to obtain moderately-sized Pt nanoparticles. Linear sweep voltammetry was employed at a current density of 5 mA/cm<sup>2</sup> and continuous negative pulse for 10 ms. After each negative pulse, a short positive pulse (current density of 5 mA/cm<sup>2</sup>, continued for 2 ms) is discharged to the barrier layer capacitance. Then t<sub>off</sub> = 100 ms time was used to restore the concentration of metal ions on the deposition surface.

**Figure 1.** Current-time curve for the preparation of Pt-doped TiO<sub>2</sub>NTs.

## 2.2. Pt-Doped TiO<sub>2</sub>NTs Sensor Production

The TiO<sub>2</sub>NTs gas sensor is different from traditional gas sensors. TiO<sub>2</sub>NTs grow directly on the surface of a metal titanium plate and are not coated on a traditional Si substrate or an Al<sub>2</sub>O<sub>3</sub> base. Therefore, high-temperature conductive silver glue was applied directly to the Pt-doped TiO<sub>2</sub>NTs surface to prepare the electrical contacts. The electrodes were closely pasted onto the TiO<sub>2</sub>NTs. Finally, the wires were connected to measure the surface resistance signal of the sensor. A sketch of the Pt-doped TiO<sub>2</sub>NTs sensor is shown in Figure 2.

**Figure 2.** Sketch of the Pt-doped TiO<sub>2</sub>NTs sensor.

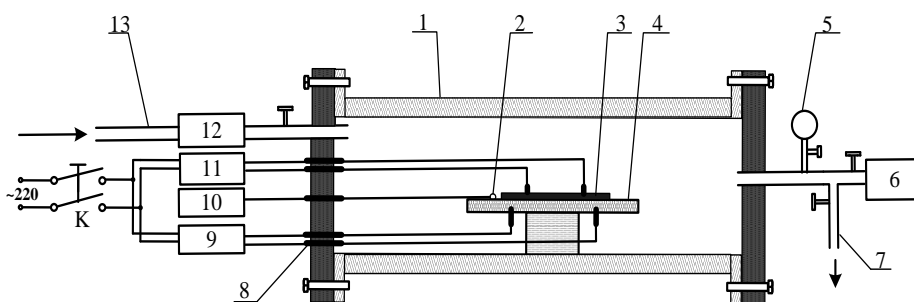
## 2.3. Gas Sensing Test Device and Method for the TiO<sub>2</sub>NTs Sensor

Figure 3 presents a schematic of the device utilized to measure the TiO<sub>2</sub>NTs sensor's response to the SF<sub>6</sub> gas decomposition products. In the experiment, the calibration gases of the SF<sub>6</sub> decomposition products were injected through the air intake. The gas flow meter controls and detects the flow rate of the measured gas, and the ceramic heater chip and thermal resistance probe control and measure the surface sensor temperature. The TiO<sub>2</sub>NTs sensor was then placed in a sealed quartz glass tube. The resistance characteristics of the sensor were determined with an impedance analyzer, and the resistance value of the entire process was recorded. The relative changes in the TiO<sub>2</sub>NTs sensor's resistance (*i.e.*, sensitivity) was calculated with the formula:

$$R\% = \frac{(R - R_0)}{R_0} \times 100\%$$

where  $R$  is the sensor resistance value after injecting the detected gas, and  $R_0$  is the stable resistance in  $N_2$ . The response time of the sensor is the time when the sensor's resistance reached 90% of the maximum value.

**Figure 3.** Detection test device utilized to measure the  $TiO_2NTs$  sensor's response to the  $SF_6$  decomposition products. (1) Quartz glass tube; (2) thermal resistance probe; (3) carbon NT sensor; (4) ceramic heating slices; (5) vacuum form; (6) vacuum pump; (7) ventilation ducts; (8) terminals; (9) AC regulator; (10) temperature display apparatus; (11) impedance analyzer; (12) gas flow meter and (13) inlet ducts.



The adsorption of the  $TiO_2NTs$ , air oxygen, and water vapor was considered. Dynamic measurements were performed in the experimental method to exclude the impact of these factors [11]. The concrete steps are as follows: prior to the gas sensing response experiment, high-purity  $N_2$  was injected at a flow rate of 0.1 L/min. The power supply of the heating sheet was turned on simultaneously. The regulator knob was adjusted to control the temperature of the sensor surface (to maintain the desired temperature) until the  $TiO_2NTs$  sensor resistance value stabilized. The value was recorded as  $R_0$ . Next, one of the gaseous  $SF_6$  decomposition products, namely,  $SO_2$ , was injected. The gas flow rate in the device should be consistent with the injection rate for  $N_2$ . The sensor's resistance changed distinctly and achieved stability quickly (fluctuation near one resistance). The resistance value in this process was recorded as  $R$ . Lastly, high-purity  $N_2$  was injected at a flow rate of 0.1 L/min when the resistance of the sensor was stable; this procedure was performed until the resistance of the sensor gradually stabilized at a certain value. The value was recorded as  $R_0$ .

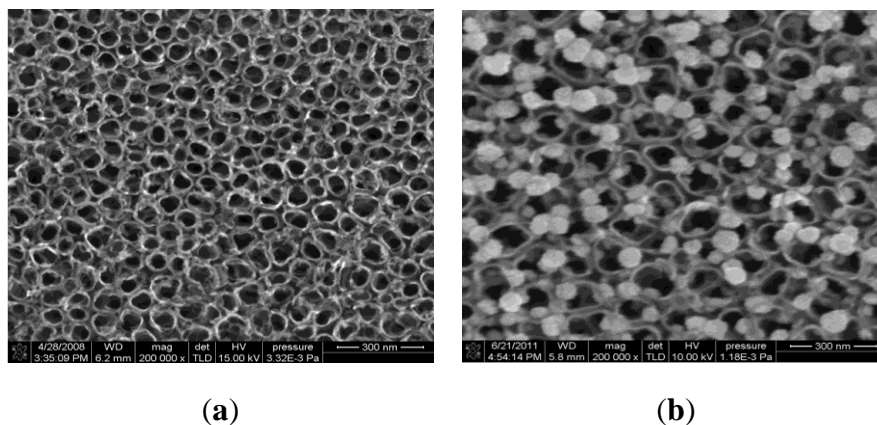
### 3. Results and Discussion

#### 3.1. Morphology of the Pt-Doped $TiO_2NTs$ Obtained through Characterization and Analysis

A JEOL JSM-7000 field emission scanning electron microscope (SEM, JEOL, Japan) with an accelerating voltage of 10 kV was used to observe the sample. Figure 4 shows the SEM images of the intrinsic and Pt-doped  $TiO_2NTs$  prepared by anodic oxidation and the proposed experimental method, respectively. Figure 4a shows the intrinsic  $TiO_2NTs$ , and Figure 4b shows the Pt-doped  $TiO_2NTs$ . The nanoparticles loaded between the tube and pipe in the Pt-doped  $TiO_2NTs$  are Pt nanoparticles. The SEM

images show that TiO<sub>2</sub>NTs prepared by the proposed experimental method are moderately sized and evenly distributed, thereby achieving the desired effect.

**Figure 4.** SEM images of the intrinsic and Pt-doped TiO<sub>2</sub>NTs. (a) Intrinsic TiO<sub>2</sub>NTs. (b) Pt-doped TiO<sub>2</sub>NTs.



XRD was performed to analyze the sensor and to further validate whether the white nanoparticles in the SEM images are Pt [13]. The results are shown in Figure 5.

**Figure 5.** XRD of the Pt-doped TiO<sub>2</sub>NTs.

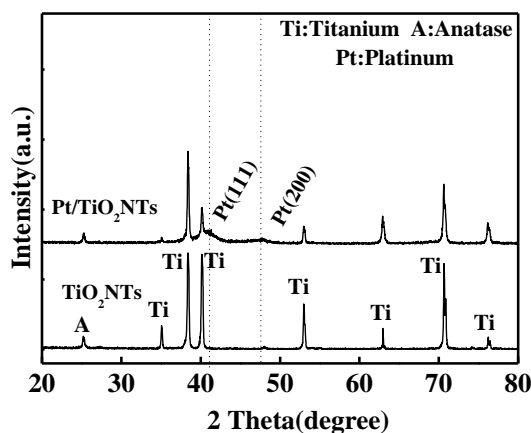


Figure 5 shows that a strong anatase (101) crystal plane peak exists at  $2\theta = 25.3^\circ$  (A in the figure) in the intrinsic and Pt-doped TiO<sub>2</sub>NTs. In the XRD pattern of the Pt-doped TiO<sub>2</sub>NTs, a Pt (111) and a Pt (200) crystal surface peak exist at  $2\theta = 40.5^\circ$  and  $2\theta = 46^\circ$ , respectively. The XRD pattern of the intrinsic TiO<sub>2</sub>NTs did not have this peak. This result shows that pulsed electrodeposition is useful when Pt-doped nanoparticles are utilized with intrinsic TiO<sub>2</sub>NTs.

### 3.2. Influence of Operating Temperature on the Gas Sensitivity Characteristics of the Pt-Doped TiO<sub>2</sub>NTs Sensor

The performance of the metal oxide semiconductor gas-sensitive material is greatly influenced by the operating temperature. Metal or non-metal doping has a significant impact on the temperature characteristics of the metal oxide semiconductor material, therefore, examining the gas sensing response

of Pt-doped  $\text{TiO}_2\text{NTs}$  sensors to the  $\text{SF}_6$  partial discharge decomposition products ( $\text{SOF}_2$ ,  $\text{SO}_2\text{F}_2$ ,  $\text{SO}_2$  gas) is necessary in determining the optimum operating temperature of the sensor. The prepared Pt-doped  $\text{TiO}_2\text{NTs}$  sensor was placed in the test device described earlier (Figure 3). The surface of the sensor was then heated, and the temperature of the surface was controlled with the temperature control device. The gas sensing characteristics of the Pt-doped  $\text{TiO}_2\text{NTs}$  sensor were tested in 50 ppm  $\text{SOF}_2$  and  $\text{SO}_2\text{F}_2$  gas whose surface temperature changes from 20 °C to 240 °C. The result is shown in Figure 6.

**Figure 6.** Sensitivity of the Pt-doped and intrinsic  $\text{TiO}_2\text{NTs}$  sensors at different operating temperatures.

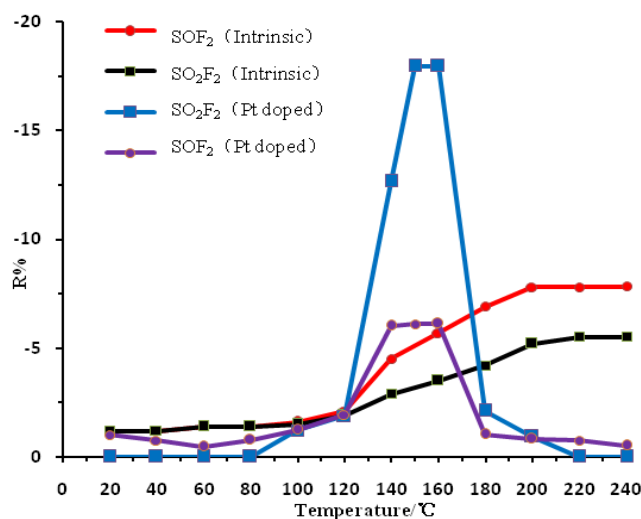


Figure 6 shows the curve of the change in the resistance of the Pt-doped and intrinsic  $\text{TiO}_2\text{NTs}$  gas sensors in response to the  $\text{SF}_6$  decomposition component gases  $\text{SOF}_2$  and  $\text{SO}_2\text{F}_2$ . The figure shows that the gas response value of the intrinsic  $\text{TiO}_2\text{NTs}$  sensor to the  $\text{SF}_6$  decomposition product gases (*i.e.*, resistance change rate; R%) increases with the increase in the sensor surface temperature. The saturation temperature is approximately 200 °C, which is thus the intrinsic  $\text{TiO}_2\text{NTs}$  sensor's optimum operating temperature. The R% of the Pt-doped  $\text{TiO}_2\text{NTs}$  sensor also increases with the increase in the sensor surface temperature. The largest response value is generated when the temperature reaches 140 °C to 160 °C. As the temperature continuously increases the sensor response values begin to decline sharply. The response value becomes small when the temperature reaches 240 °C. This result indicates that the optimum operating temperature for the intrinsic  $\text{TiO}_2\text{NTs}$  sensor is approximately 150 °C. This finding indicates that the Pt-doped nanoparticles not only reduces the optimal operating temperature of the sensor, but also changes the temperature characteristic curve significantly. Because the Pt doped sensor and  $\text{SF}_6$  decomposition products undergo redox reactions the sensor resistance decreases and the response values are negative. A detailed explanation can be found below in Section 3.4. When the intrinsic  $\text{TiO}_2\text{NTs}$  sensor has reached the optimum operating temperature, the response remains unchanged even with a continuous increase in temperature, possibly because the gas sensor surface adsorption and desorption rates reach a dynamic equilibrium and thus, the sensor response remains unchanged.

The sensor surface microstructure and charge distribution is changed after the Pt nanoparticles are doped on it [14]. When the surface temperature of the  $\text{TiO}_2\text{NTs}$  is higher than the optimum operating temperature, the Pt-doped nanoparticles improve the chemical desorption rate of the sensor surface. This

phenomenon causes the desorption rate of the chemical adsorption of oxygen to be greater than its adsorption rate; the surface oxygen chemical adsorption density decreases, causing the response value of the sensor to decrease rapidly.

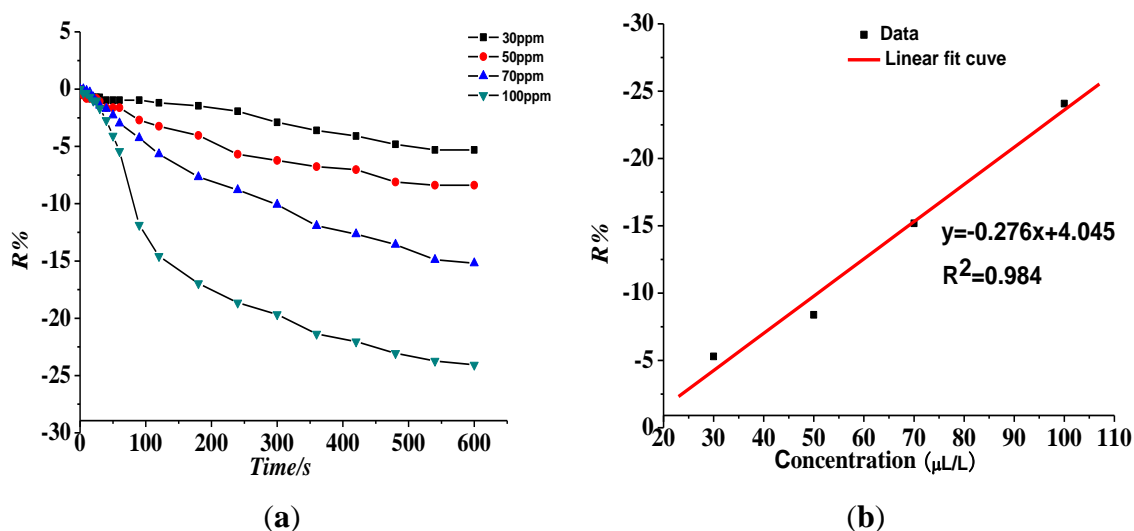
### 3.3. Response of the Gas-Sensitive Characteristics of the Pt-Doped TiO<sub>2</sub>NTs Sensor to SF<sub>6</sub> Decomposition Component Gas

The sensor operating temperature was 150 °C. The gas-sensitive response curve of the Pt-doped TiO<sub>2</sub>NTs sensor was tested with SO<sub>2</sub>, SOF<sub>2</sub>, and SO<sub>2</sub>F<sub>2</sub> gases at 30, 50, 70, and 100 ppm. The change rate in the sensor's resistance at various concentrations, *i.e.*, gas sensing response values, was calculated. The linear relationship between the change rate in the sensor's resistance and the gas concentration was investigated by the linear fitting based on the results. The concentration of the measured gas was also estimated by curve fitting based on the response value of the sensor.

(1) Response of the gas-sensing characteristics of the Pt-doped TiO<sub>2</sub>NTs gas sensor to SF<sub>6</sub> partial discharge decomposition component SO<sub>2</sub>.

Figure 7 shows that the resistance of the Pt-doped TiO<sub>2</sub>NTs sensor to 30, 50, 70, and 100 ppm of SO<sub>2</sub> gas is 5.31%, 8.38%, 15.18%, and 24.07%, respectively. The linear fit function between R% and SO<sub>2</sub> gas concentration is  $y = 0.276x + 4.045$ , and linear correlation coefficient R<sup>2</sup> is 0.984.

**Figure 7.** Response of the Pt-doped TiO<sub>2</sub>NTs sensor to different concentrations of SO<sub>2</sub> at 150 °C operating temperature. (a) Response of the sensor's gas-sensing characteristics to different concentrations of SO<sub>2</sub>; (b) Linear relationship between sensor response and gas concentration.

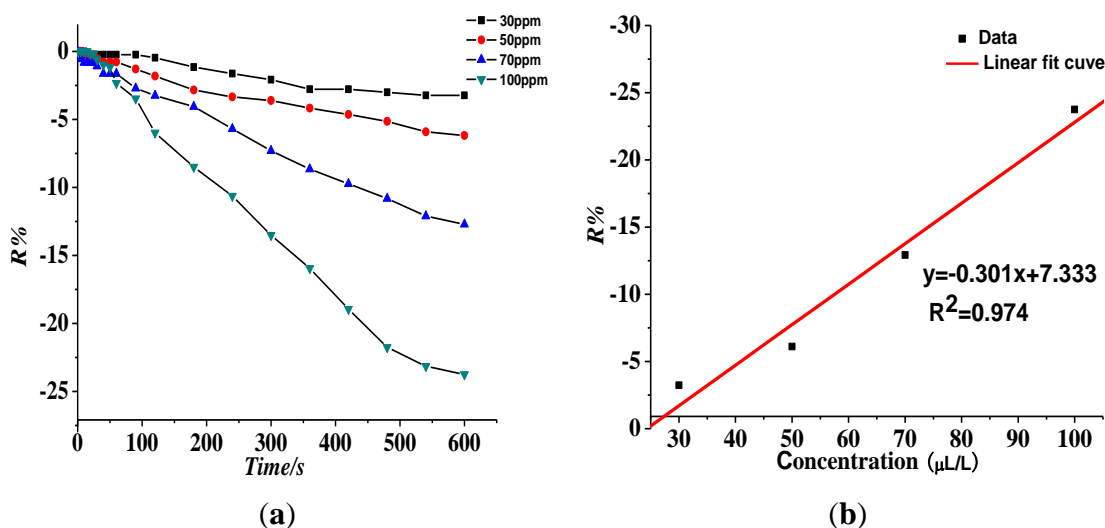


(2) Response of the gas sensing characteristics of the Pt-doped TiO<sub>2</sub>NTs gas sensors to SF<sub>6</sub> partial discharge decomposition component SOF<sub>2</sub>

Figure 8 shows the Pt-doped TiO<sub>2</sub>NTs gas sensor's gas-sensing response curve to 30, 50, 70, and 100 ppm of SOF<sub>2</sub> at 150 °C. Figure 8a shows that the resistance change rate with increasing concentration is 3.23%, 6.11%, 12.92%, and 23.75% at different tested concentrations of SOF<sub>2</sub>. The fitting curve is shown in Figure 8b. The linear fit function is  $y = 0.301x + 7.333$ , and linear correlation

coefficient  $R_2$  is 0.974. This result shows that at a certain concentration range, a linear relationship exists between  $R\%$  and  $\text{SO}_2\text{F}_2$  gas concentration.

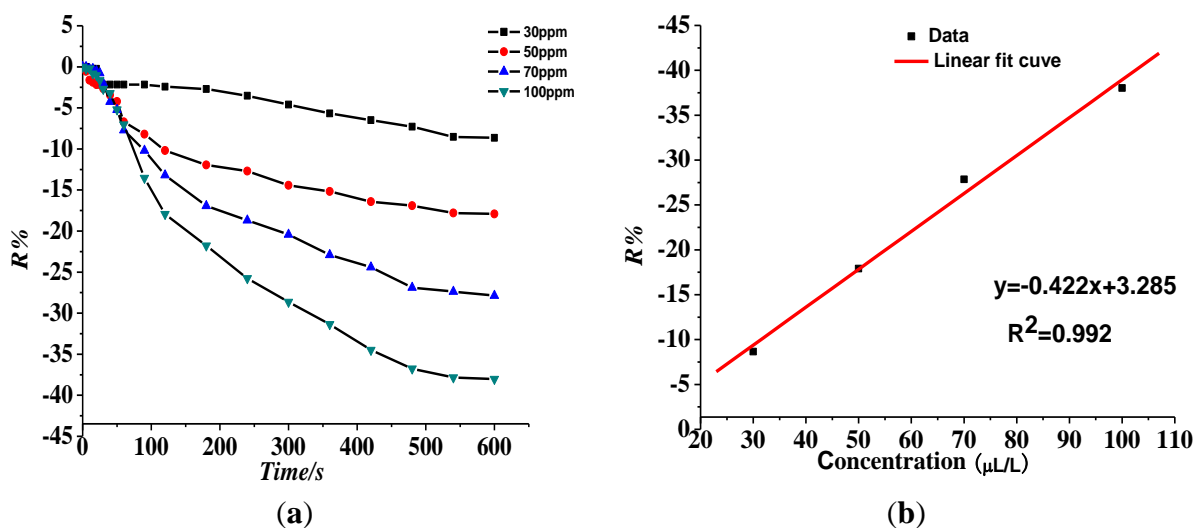
**Figure 8.** Response of the Pt-doped  $\text{TiO}_2\text{NTs}$  sensor to different concentrations of  $\text{SO}_2\text{F}_2$  at 150 °C operating temperature. (a) Response of the sensor's gas-sensing characteristics to different concentrations of  $\text{SO}_2\text{F}_2$ ; (b) Linear relationship between sensor response and gas concentration.



(3) Response of the gas-sensing characteristics of the Pt-doped  $\text{TiO}_2\text{NTs}$  gas sensor to  $\text{SF}_6$  partial discharge decomposition component  $\text{SO}_2\text{F}_2$ .

Figure 9 shows that the resistance of the Pt-doped  $\text{TiO}_2\text{NTs}$  sensor to 30, 50, 70, and 100 ppm of  $\text{SO}_2\text{F}_2$  gas is 8.65%, 17.91%, 27.86%, and 38.02%, respectively. The fitting curve is shown in Figure 8b. The linear fit function is  $y = 0.422x + 3.285$ , and linear correlation coefficient  $R_2$  is 0.992.

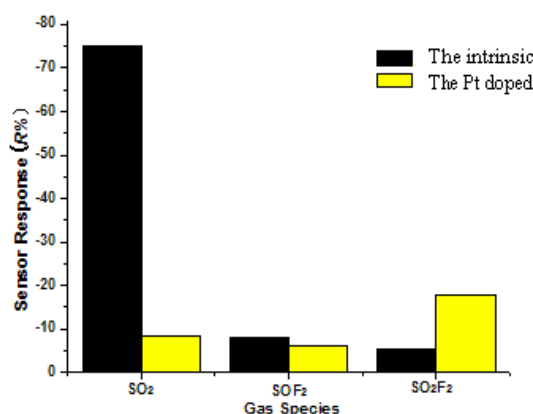
**Figure 9.** Response of the Pt-doped  $\text{TiO}_2\text{NTs}$  sensor to different concentrations of  $\text{SO}_2\text{F}_2$  at 150 °C operating temperature. (a) Response of the sensor's gas-sensing characteristics to different concentrations of  $\text{SO}_2\text{F}_2$ ; (b) Linear relationship between sensor response and gas concentration.



### 3.4. Discussion on the Mechanism of the TiO<sub>2</sub>NTs Sensor's Gas Response Sensitivity

Figure 10 provides a comparison of the gas response of the intrinsic and Pt-doped TiO<sub>2</sub>NTs gas sensors to 50 ppm of the three SF<sub>6</sub> decomposition productt gases (SO<sub>2</sub>, SOF<sub>2</sub>, SO<sub>2</sub>F<sub>2</sub>) at the optimal operating temperature. The gas response of the intrinsic TiO<sub>2</sub>NTs sensor to the three decomposition gases is discussed in Reference [12]. We find that the R% response value of the intrinsic and Pt-doped TiO<sub>2</sub>NTs to the three SF<sub>6</sub> decomposition component gases is negative. This finding indicates that after the three gases were injected separately, the resistance of the intrinsic and Pt-doped TiO<sub>2</sub>NTs decreased, however, the three response values are different in size.

**Figure 10.** Response of the Pt-doped and intrinsic TiO<sub>2</sub>NTs to different SF<sub>6</sub> decomposition components.



TiO<sub>2</sub> is an N-type semiconductor and has many oxygen vacancies, thus, its gas sensitive effect is obvious and is generally considered a surface adsorption-controlled mechanism. Its response to the measured gas is caused by the chemisorption reaction between oxygen in the air and the TiO<sub>2</sub>NTs sensor surface. Oxygen ions exist in the grain boundaries between grains, thereby causing the grain boundary barrier to become higher, thus, the resistance of the TiO<sub>2</sub>NTs sensor increases, blocking the transfer of the carriers. When meeting the reducing gas or the electron supply gas, an oxidation reduction occurs between the surface adsorbed oxygen ions and the reducing gas. The number of adsorbed oxygen ions decreases sharply, the sensor surface potential barrier is reduced, carrier shifting is promoted, TiO<sub>2</sub> resistance is reduced, and the gas sensing response is finally achieved.

Figure 10 shows that the R% response values of the intrinsic and Pt-doped TiO<sub>2</sub>NTs to the three SF<sub>6</sub> decomposition component gases are negative. This result means that the resistance of the intrinsic and Pt-doped TiO<sub>2</sub>NTs decreased. The response mechanism shows that the three measured gases function as a reducing gas or an electron-donating gas. The reaction occurs as follows:



where R is one of SF<sub>6</sub> decomposition component gases, and O<sub>ads</sub><sup>-</sup> pertains to the oxygen ions adsorbed by the sensor surface.

The gas-sensing responses of the intrinsic TiO<sub>2</sub>NTs to the three tested gas are SO<sub>2</sub> (74.6%) > SOF<sub>2</sub> (7.82%) > SO<sub>2</sub>F<sub>2</sub> (5.52%). This finding shows that the decreasing electron supply of SO<sub>2</sub> gas is the strongest in the above-mentioned micro-oxidation reduction reaction (*i.e.*, the most likely to lose electrons), and the supply of SOF<sub>2</sub> and SO<sub>2</sub>F<sub>2</sub> gas is the weakest. The selectivity of the sensor is

best for SO<sub>2</sub> gas. The gas-sensing response of the Pt-doped TiO<sub>2</sub>NTs to the three tested gases is SO<sub>2</sub>F<sub>2</sub> (17.91%) > SO<sub>2</sub> (8.38%) > SOF<sub>2</sub> (6.11%). The Pt-doped TiO<sub>2</sub>NTs sensor's response (*i.e.*, the selectivity of the sensor changes) to the three SF<sub>6</sub> decomposition component gases (SO<sub>2</sub>, SOF<sub>2</sub>, SO<sub>2</sub>F<sub>2</sub>) changes significantly.

When the metal catalyst is doped, Pt functions as an oxygen storage point, such that it constantly provides O<sub>ads</sub><sup>-</sup> to the TiO<sub>2</sub>NTs sensor surface. Noble metal doping decreases the O<sub>2</sub> + e<sup>-</sup> → 2 O<sub>ads</sub><sup>-</sup> activation energy, thus, the optimum operating temperature point also decreases, and the reaction rate and gas sensitive effects are enhanced. As the catalyst particles on the surface of TiO<sub>2</sub> sensitive body have a significant affinity interaction with the gas to be measured, the gas is attached firmly to the sensor's surface at a low temperature. The gas will "migrate" from the catalyst particles to the surface of the sensitive body and react with the adsorbed oxygen ions. Ultimately, the sensitivity of the gas sensor increases, and the sensor response rate is accelerated [15].

The three sulfide gases tested were SO<sub>2</sub>, SOF<sub>2</sub>, and SO<sub>2</sub>F<sub>2</sub>. Sulfides have a specific degree of toxicity to a noble metal catalyst, and the level of toxicity is related to sulfide valence and molecular structure. The toxicity of the three experimental gases from the strongest to the weakest is SO<sub>2</sub> > SOF<sub>2</sub> > SO<sub>2</sub>F<sub>2</sub>. S<sup>6+</sup> within a certain range is non-toxic [16]. When the toxicity of SO<sub>2</sub> passes through, the Pt-doped TiO<sub>2</sub>NTs sensor is poisoned. The specific process is as follows: First, SO<sub>2</sub> is physical adsorbed on the active center of the catalyst; Second, a redox reaction occurs in the SO<sub>2</sub> with the active ingredient; Third, the reaction produces the corresponding alkylene sulfide and sulfides, which block the active sites. The catalyst activity decreases in this complex series of processes [16]. The sensitivity of the almost non-toxic SO<sub>2</sub>F<sub>2</sub> is greatly improved. The sensitivity of SOF<sub>2</sub> is almost unchanged [12].

### 3.5. Recovery Test for the Pt-Doped TiO<sub>2</sub>NTs Sensor

The recovery of the sensor in one of the SF<sub>6</sub> decomposition product gases (SO<sub>2</sub>) at 150 °C was tested. The test results are shown in Figure 11. The sensor's resistance changed significantly when 50 ppm of SO<sub>2</sub> gas was injected. When the sensor's resistance stabilized, pure N<sub>2</sub> gas was injected. The sensor's resistance increased gradually, but did not revert to the initial resistance value. The above experimental procedure was repeated when the resistance value of the sensor stabilized again. The sensitivity of the sensor decreased greatly; the resistance value did not revert to the initial value, which indicates that the sensor underwent chemical poisoning. Afterward, irradiation with ultraviolet light was performed, and N<sub>2</sub> gas was injected again. The resistance value of the sensor gradually increased and ultimately reverted to the initial value and became stable. When 50 ppm of SO<sub>2</sub> gas was injected, the sensitivity of the sensor returned to its level in the first test. Although S<sup>4+</sup> is toxic to the Pt-doped TiO<sub>2</sub>NTs sensor and may affect the initial resistance and sensitivity of the sensor, UV light irradiation resolves this problem by allowing sulfide ion desorption.

The recovery of the sensor in one of the SF<sub>6</sub> decomposition product gases (SO<sub>2</sub>F<sub>2</sub>) at 150 °C was tested. The test results are shown in Figure 12.

This phenomenon is due to the residual thermal decomposition of SO<sub>2</sub>F<sub>2</sub> molecules fixed in the TiO<sub>2</sub> nanotube arrays as the result of chemical adsorption. The adsorption energy of chemical adsorption is much larger than the physical adsorption capacity. Therefore, ultraviolet light is used to desorb SO<sub>2</sub>F<sub>2</sub> molecules attached on the sensor. The forbidden bandwidth of the ultraviolet photon energy is almost the same as that of many metal oxide semiconductors, hence ultraviolet radiation can be absorbed

effectively by the TiO<sub>2</sub>NTs. The surface of the film and the inner portion undergo a range of physical and chemical processes. In the case of gas adsorption, ultraviolet radiation can be absorbed by the TiO<sub>2</sub>NTs through electron-hole pair excitation, thus increasing the carrier concentration and reducing the grain interface barrier. Through these processes, the TiO<sub>2</sub>NTs conductivity can be increased, and the resistor reduced. Ultraviolet radiation can be absorbed directly by gas molecules to produce desorption or stimulate chemical reactions between different types of molecules [17]. This method can improve sensor repeatability and reduce sensor chemical poisoning [12]. The recovery curve of SOF<sub>2</sub> is very similar to that of SO<sub>2</sub>F<sub>2</sub>, so in the paper we do not repeat the corresponding discussion.

**Figure 11.** Recovery curve of the Pt-doped TiO<sub>2</sub>NTs sensor to SO<sub>2</sub>.

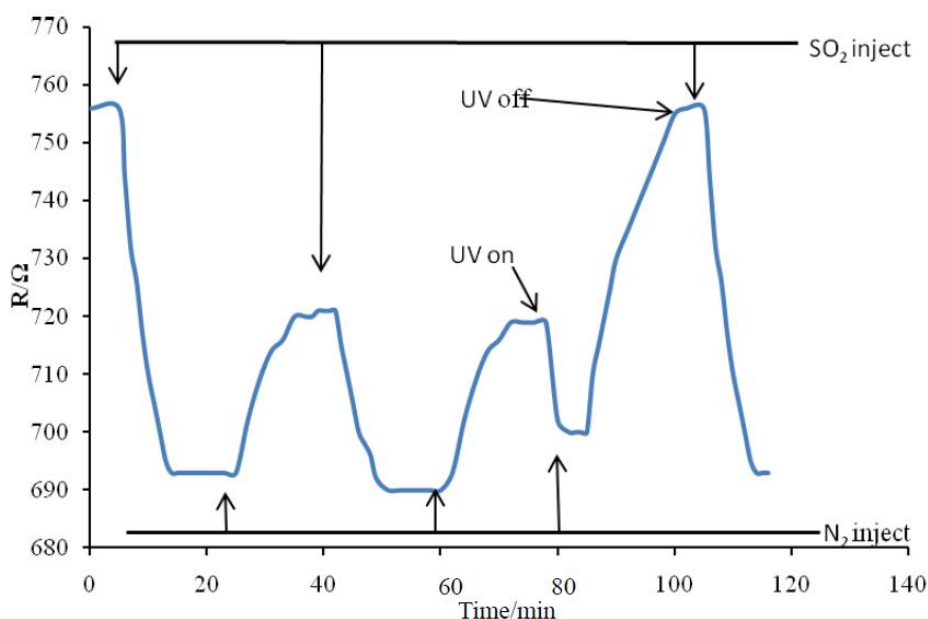
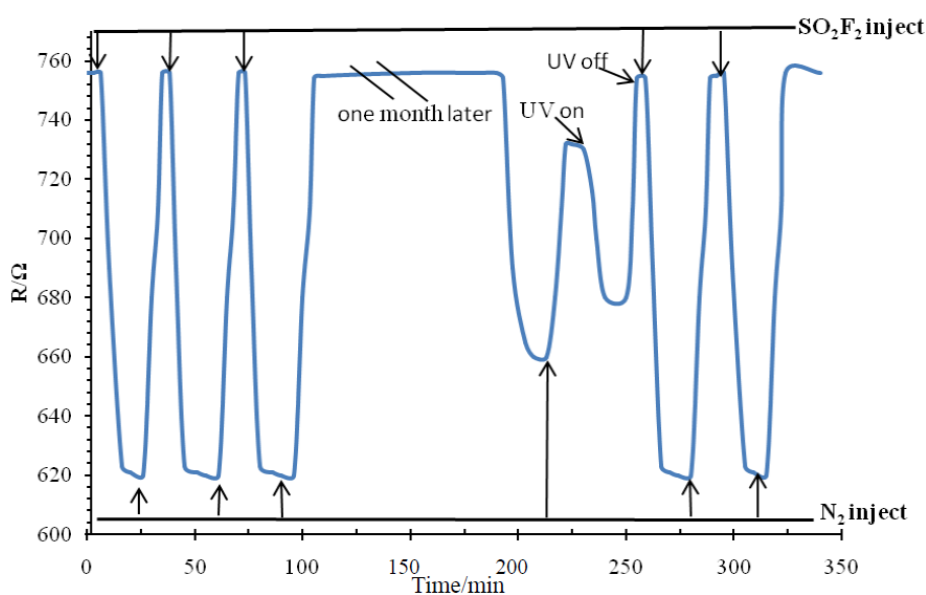


**Figure 12.** Recovery curve of the Pt-doped TiO<sub>2</sub>NTs sensor to SO<sub>2</sub>F<sub>2</sub>.



#### 4. Conclusions

A Pt-doped TiO<sub>2</sub>NTs sensor was prepared by pulse electrodeposition; the sensor is based on an intrinsic TiO<sub>2</sub>NTs sensor prepared by anodic oxidation. The temperature characteristics of the Pt-doped TiO<sub>2</sub>NTs sensor were analyzed, and the gas sensing properties of three SF<sub>6</sub> decomposition product gases were determined through experiments on their gas sensing properties. The gas sensing characteristics of the Pt-doped TiO<sub>2</sub>NTs sensor were compared with those of the intrinsic TiO<sub>2</sub>NTs sensor. The response mechanism was also discussed. The following conclusions were obtained:

- (1) Under similar conditions, the Pt-doped TiO<sub>2</sub>NTs sensor's response to SO<sub>2</sub>F<sub>2</sub> is strong, and its response to SOF<sub>2</sub> and SO<sub>2</sub> is weak. This result means that the Pt-doped TiO<sub>2</sub>NTs sensor exhibits good selectivity to SO<sub>2</sub>F<sub>2</sub> gas.
- (2) The temperature characteristic curve of the Pt-doped TiO<sub>2</sub>NTs sensor is different from that of the intrinsic TiO<sub>2</sub>NTs sensor. The optimum operating temperature of the Pt-doped TiO<sub>2</sub>NTs sensor is approximately 150 °C. When the temperature increases to 200 °C, the sensitivity response of the sensor declines sharply. When the temperature reaches 240 °C, the response value is very small (essentially zero).
- (3) Comparative analysis of the gas sensing properties of the Pt-doped and intrinsic TiO<sub>2</sub>NTs sensors indicates that the Pt-doped nanoparticles change the gas sensing response of the intrinsic TiO<sub>2</sub>NTs sensor (*i.e.*, the selectivity of the sensor) to the three SF<sub>6</sub> decomposition component gases. A preliminary discussion of the response mechanism of the Pt-doped TiO<sub>2</sub>NTs sensor was presented.

#### Acknowledgments

We gratefully acknowledge the financial support from China National Natural Science Foundation (51277188), program for China New Century Excellent Talents (NCET-12-0590) and project No. 0213005202042 supported by the Fundamental Research Funds for the Central Universities, in China.

#### Conflicts of Interest

The authors declare no conflict of interest.

#### References

1. Beyer, C.; Jenett, H.; Kföckow, D. Influence of reactive SF<sub>6</sub> gases on electrode surfaces after electrical discharges under SF<sub>6</sub> atmosphere. *IEEE Trans. Dielectr. Electr. Insul.* **2000**, *7*, 234–240.
2. Christophorou, L.G.; Olthoff, J.K. Electron interactions with SF<sub>6</sub>. *J. Phys. Chem. Ref. Data* **2000**, *29*, 267–330.
3. Kurte, R.; Heise, H.M.; Klockow, D. Quantitative infrared spectroscopic analysis of SF<sub>6</sub> decomposition products obtained by electrical partial discharges and sparks using PLS-calibrations. *J. Mol. Struct.* **2001**, *565*, 505–513.
4. Suehiro, J.; Zhou, G.; Hara, M. Detection of partial discharge in SF<sub>6</sub> gas using a carbon NTs based gas sensor. *Sens. Actuators B* **2005**, *2*, 164–169.

5. Zhang, X.X.; Liu, W.T.; Tang, J.; Xiao, P. Study on PD detection in SF<sub>6</sub> using multi-wall carbon NTs gas sensor. *IEEE Trans. Dielectr. Electr. Insul.* **2010**, *17*, 833–838.
6. Piemontesi, M.; Niemeyer, L. Sorption of SF<sub>6</sub> and SF<sub>6</sub> Decomposition Products by Activated Alumina and Molecular Sieve 13×. In Proceedings of IEEE International Symposium on Electrical Insulation, Montreal, QC, Canada, 16–19 June 1996.
7. Mor, G.K.; Varghese, O.K.; Paulose, M.; Shankar, K.; Grimes, C.A. A review on highly ordered, vertically oriented TiO<sub>2</sub> nanotube arrays: Fabrication, material properties, and solar energy applications. *Solar Energy Mater. Solar Cells* **2006**, *90*, 2011–2075.
8. Mor, G.K.; Shankar, K.; Paulose, M.; Varghese, O.K.; Grimes, C.A. Enhanced photocleavage of water using Titania NTs. *Nano Lett.* **2005**, *5*, 191–195.
9. Grimes, C.A.; Mor, G.K. *TiO<sub>2</sub>NT Arrays Synthesis, Properties, and Applications*; Springer: Norwell, MA, USA, 2009.
10. Yun, H. Preparation of NO<sub>2</sub> Gas Sensor Based on TiO<sub>2</sub>NTs. M.Sc. Thesis, Dalian University of Technology, Dalian, China, 2005.
11. Varghese, O.K.; Gong, D.; Paulose, M.; Ong, K.G.; Grimes, C.A. Hydrogen sensing using Titania NTs. *Sens. Actuators B* **2003**, *93*, 338–344.
12. Zhang, X.X.; Zhang, J.B.; Tang, J.; Jia, Y.C.; Xiao, P. TiO<sub>2</sub>NTs sensor for detecting SF<sub>6</sub> decomposition component SO<sub>2</sub>. *Sensors* **2012**, *12*, 3302–3313.
13. He, H.C.; Xiao, P.; Zhou, M. Zhang, Y.H.; Jia, Y.C.; Yu, S.J. Preparation of well-distributed Pt-Ni nanoparticles on/into TiO<sub>2</sub>NTs by pulse electrodeposition for methanol photoelectro-oxidation. *Catal. Commun.* **2011**, *16*, 140–143.
14. Han, Y. The Nature of Pt/TiO<sub>2</sub> Interfacial Interaction and its Role in Catalytic Dissociation of Methanol from First Principles Theory. Ph.D. Thesis, Tianjin University, Tianjin, China, 2007.
15. Gangal, N.D.; Gupta, N.M.; Lyster, R.M. Microcalorimetric study of the interaction of CO, O<sub>2</sub>, and CO + O<sub>2</sub> with Pt/SnO<sub>2</sub> and SO<sub>2</sub> catalysts. *J. Catal.* **1990**, *11*, 13–25.
16. Yang, H.P.; Qiu, F.L.; Lu, S.J. Studies on mechanism of SO<sub>2</sub> poisoning of non-noble metal. *Environ. Chem.* **1992**, *1*, 19–23.
17. Sun, J.P.; Hui, C.; Xu, A.L.; Liu, H.W. Progress in research on gas-sensing properties of metal oxide thin films under UV irradiation. *Electron. Compon. Mater.* **2005**, *24*, 65–68.

© 2013 by the authors; licensee MDPI, Basel, Switzerland. This article is an open access article distributed under the terms and conditions of the Creative Commons Attribution license (<http://creativecommons.org/licenses/by/3.0/>).